AD-A082 046 SUSSEX UNIV BRIGHTON (ENGLAND) SCHOOL OF ENGINEERING--ETC F/G 11/6
SUPERPLASTICITY IN SPLAT-QUENCHED PB-SN EUTECTIC.(U)
JAN 80 R CHEESE, B CANTOR N00014-78-G-0048
UNCLASSIFIED TR-5 NL

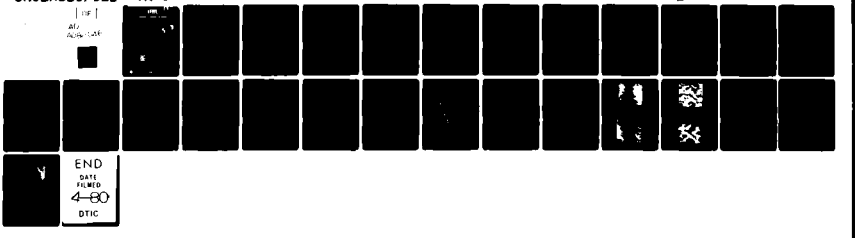

END
DATE FILMED
4-80
DTIC

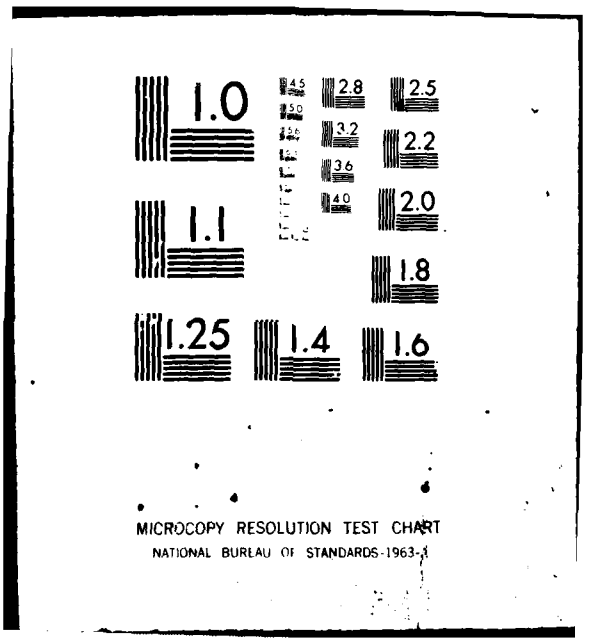
1.0
1.1
1.25
1.4
1.6
1.8
2.0
2.2
2.5
2.8
3.2
3.6
4.0
4.5
5.0
MICROCOPY RESOLUTION TEST CHART
NATIONAL BUREAU OF STANDARDS-1963-A

SECURITY CLASSIFICATION OF THIS PAGE (When Data Entered)

REPORT DOCUMENTATION PAGE

READ INSTRUCTIONS BEFORE COMPLETING FORM

1. REPORT NUMBER: Technical Report No. 5
2. GOVT ACCESSION NO.:
3. RECIPIENT'S CATALOG NUMBER:

4. TITLE (and Subtitle): Superplasticity in Splat-Quenched Pb-Sn Eutectic
5. TYPE OF REPORT & PERIOD COVERED: Technical Report
6. PERFORMING ORG. REPORT NUMBER:

7. AUTHOR(s): R. Cheese and B. Cantor
8. CONTRACT OR GRANT NUMBER(s): N00014-78-G-0048

9. PERFORMING ORGANIZATION NAME AND ADDRESS: School of Engineering & Applied Sciences, University of Sussex, Brighton, UK.
10. PROGRAM ELEMENT, PROJECT, TASK AREA & WORK UNIT NUMBERS:

11. CONTROLLING OFFICE NAME AND ADDRESS: Metallurgy Branch, Office of Naval Research, Arlington, VA22217
12. REPORT DATE: 1st January 1980
13. NUMBER OF PAGES: 26

14. MONITORING AGENCY NAME & ADDRESS (if different from Controlling Office): TR-5
15. SECURITY CLASS. (of this report): Unclassified
15a. DECLASSIFICATION/DOWNGRADING SCHEDULE:

16. DISTRIBUTION STATEMENT (of this Report): Unlimited

17. DISTRIBUTION STATEMENT (of the abstract entered in Block 20, if different from Report):

18. SUPPLEMENTARY NOTES: To be published in Materials Science and Engineering

19. KEY WORDS (Continue on reverse side if necessary and identify by block number): Melt-spinning, splat-quenching, crystallisation, eutectic, superplasticity

20. ABSTRACT (Continue on reverse side if necessary and identify by block number):

This paper described the microstructure and mechanical properties of Pb-Sn eutectic alloys prepared by melt-spinning

DD FORM 1 JAN 73 1473 EDITION OF 1 NOV 65 IS OBSOLETE
S/N 0102-LF-014-6601

SECURITY CLASSIFICATION OF THIS PAGE (When Data Entered)

411513

SUPERPLASTICITY IN SPLAT-QUENCHED Pb-Sn EUTECTIC

by

R. Cheese and B. Cantor

School of Engineering & Applied Sciences
University of Sussex
Falmer, Brighton, Sussex, UK.

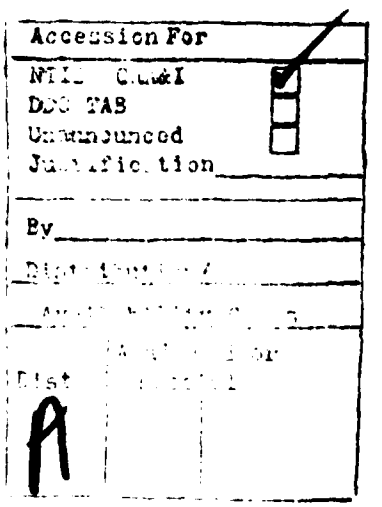

Abstract

Lead-tin eutectic alloy tapes have been prepared by melt-spinning over a wide range of solidification conditions. In all cases, the rapid solidification produces a microstructure consisting of equiaxed lead-rich and tin-rich grains, approximately 4μm in size. This microstructure could result from a divorced eutectic solidification process, or, more likely, from post-solidification coarsening. Under tensile loading, the melt-spun lead-tin eutectic tapes exhibit superplastic deformation with large failure strains, a sigmoidal variation of log flow stress with log flow strain, a strain rate sensitivity of ~ 0.42, and an activation energy for superplastic flow of $\sim 54 KJ\ mole^{-1}$.

Introduction

Since the work of Duwez et al (1,2) there has been considerable scientific interest in the structure and properties of splat-quenched alloys (3-7). Liquid alloy droplets have been splat-quenched at cooling rates of $\gtrsim 10^5 Ks^{-1}$ usually by either the gun technique (8) in which the liquid is projected onto a solid substrate, or a piston technique (9) in which the liquid is squeezed between two solid surfaces. Depending upon the particular alloy system. splat-quenching can produced amorphous structures (1,10), metastable crystalline phases (9,11), extended solubility (12,13), anomalous vacancy concentrations (14,15), or suppression of martensite formation (16-18). In many cases, these novel microstructures have been shown to have potentially useful electrical, magnetic, mechanical, or electrochemical properties (3-7,19,20).

In recent years a variety of amorphous alloys have been prepared by a new technique called chill-block casting or melt-spinning (21,22) in which a stream of liquid is solidified in contact with the outer edge of a rotating drum to produce a continuous splat-quenched solid tape. Because of the dimensional regularity of the resulting melt-spun tapes, they are particularly suitable for investigating the mechanical properties of splat-quenched alloys by conventional tensile testing (23). In addition, the cooling rate is reasonably uniform throughout the tape so that the microstructure shows less variability than is often found in specimens prepared by other splat-quenching techniques (23). The melt-spinning technique has been used almost exclusively to study amorphous alloys, and the objective of the present investigation was to extend the technique

to crystalline splat-quenched alloys using Pb-Sn eutectic as a model material. The effect of melt-spinning conditions on the solidification of Pb-Sn is described elsewhere (24); this paper describes the tensile properties of the melt-spun Pb-Sn eutectic tapes.

Experimental technique

Eutectic Pb-Sn was obtained by induction melting 99.99% pure Pb and Sn in a recrystallised alumina crucible under a dynamic argon atmosphere. Splat-quenched tapes were prepared by melt-spinning as follows. Approximately 3g of eutectic Pb-Sn was placed in a 100mm long, 9mm diameter quartz tube which narrowed to a 1mm nozzle at the bottom, and which was flushed by argon gas from the top. The alloy was induction melted and then ejected onto a highly polished 150mm diameter copper drum which was $\sim$ 1mm from the nozzle and was rotating at up to several thousand rpm. The ejection gas was argon at $\sim$ 0.01 Pa above atmospheric pressure. A series of tapes were melt-spun, typically 2-3m long and $\sim$ 1mm wide, with thicknesses depending upon the rotation rate of the copper drum. By varying the rotation rate, the surface speed of the outer edge of the drum was varied between 3-14ms^{-1} to produce tape thicknesses in the range of 30-120μm. Further details of the relationships between tape thickness and width, drum speed, ejection pressure, and nozzle diameter are given elsewhere (24).

Mechanical properties were measured in a conventional Instron tensile testing machnie. The thickness of each tensile specimen was taken from the mean of 6 micrometer measurements, the width was taken from the mean of 4 measurements with a travelling microscope, and the gauge length was measured with a vernier height gauge. Several specimens of each tape were tested. The typical gauge length was $\sim$ 100mm, and specimens were gripped at each end by being wrapped around a 35mm diameter steel capstan before being clamped into position. This gripping system was effective at preventing stress concentrations at the grips and very few specimens failed outside the gauge length. During preliminary testing at strain rates of $5.10^{-4}s^{-1}$, specimens frequently exhibited strains in excess of 100% at a steadily decreasing flow stress. This suggested that the tapes were superplastic, so in subsequent tensile tests the flow stress was measured for each tape thickness as a function of strain rate in the range 3.10^{-6} - $2.10^{-2}s^{-1}$.

This was achieved by the technique of varying the cross-head speed during tensile testing, so data was obtained at relatively small total specimen strain. To investigate the activation energy for the flow process, the variation of flow stress with strain rate was determined for two tape thicknesses over a range of temperatures from 273-373K by heating in a hot air oven. The fine scale of a splat-quenched microstructure can make it difficult to etch specimens for microscopic examination (23,25). The best results in the present experiments were obtained without etching, by observing atomic number contrast between the Pb and Sn rich phases in a Cambridge Stereoscan 2A scanning electron microscope. Specimens were examined in this way both before and after tensile deformation.

Results

Davies et al (26) have described the characteristic of superplasticity as follows. In general, the flow stress of a metal can be expressed as:

$$\sigma = K_1 \varepsilon^n \dot{\varepsilon}^m \qquad \{1\}$$

where σ is flow stress, ε strain, $\dot{\varepsilon}$ strain rate, n strain hardening exponent, m strain rate sensitivity and K_1 a constant. At temperatures below $\sim$ 0.4 times the melting point, m is small and deformation is controlled by strain hardening so that equation {1} reduces to:

$$\sigma = K_2 \varepsilon^n \qquad \{2\}$$

with K_2 approximately constant. At higher temperature, fine-grained two-phase materials exhibit a characteristic sigmoidal variation of flow stress with strain rate (see figure 1). The details of the deformation mechanisms have not yet been fully resolved. However, it is well established that at intermediate strain rates (region II) deformation is superplastic and is controlled by grain boundary sliding. In this superplastic region, the flow stress is strongly dependent upon strain rate with a strain rate sensitivity m $\gtrsim$ 0.3; the flow stress is given by:

$$\sigma = K_3 \dot{\varepsilon}^m \qquad \{3\}$$

with K_3 approximately constant. At the lowest strain rates

(region I) there is sufficient time for diffusive flow; and at the highest strain rates (region III), dislocation glide becomes important. In both cases, the strain rate sensitivity falls below 0.3.

Figure 1 shows the variation of flow stress with strain rate at room temperature for nine thicknesses of melt-spun Pb-Sn eutectic tapes. In the strain rate range $\sim 10^{-5}$-$10^{-3}s^{-1}$, the splat quenched Pb-Sn eutectic was superplastic with a strain rate sensitivity of ~ 0.4. As expected for a superplastic material, the flow stress varied sigmoidally with strain rate and the strain rate sensitivity decreased when the strain rate was either greater than $\sim 2.0.10^{-3}s^{-1}$ or less than $\sim 10^{-5}s^{-1}$. To determine whether the tape thickness had any effect on the relationship between flow stress and strain rate, equation {3} was re-written as:

$$\log \sigma = \log K_3 + m \log \dot{\varepsilon} \qquad \{4\}$$

Linear regression analysis was applied to log σ - log $\dot{\varepsilon}$ data in the strain rate range 10^{-5}-$10^{-3}s^{-1}$ to determine the correlation coefficient r, strain rate sensitivity m, and constant of proportionality K_3. The results are shown in table 1. When the regression analysis was applied separately to each of the nine tape thicknesses of 30-120μm, the room temperature strain rate sensitivity was always in the range 0.40-0.48 with a correlation coefficient >0.99. When the regression analysis was applied to the complete set of room temperature data irrespective of tape thickness, the strain rate sensitivity was 0.42; significantly, the correlation coefficient remained very high at 0.98, indicating that the variation of flow stresses with strain rate was independent of tape thickness.

At a given strain rate, the flow stress decreased as the testing temperature was raised above room temperature. Typical curves of flow stress versus strain rate are shown in figure 2 for two tape thicknesses and several temperatures. Regresssion analysis applied separately to the different temperatures and tape thicknesses showed that the strain rate sensitivity was still always in the range 0.40-0.48 and the correlation coefficeints were >0.99 (see table 1). The constant of proportionality K_3 varied with testing temperature, so it was not possible to apply a regression analysis to the complete set of data at all tape thicknesses and temperatures. However, the

different tape thicknesses tested at room temperature had a mean strain rate sensitivity of 0.42 with a standard deviation of $\pm$ 0.02 ; for the specimens tested above room temperature, the mean strain rate sensitivity was 0.43 with again a standard deviation of $\pm$ 0.02 (see table 1) confirming that the strain rate sensitivity was constant within $\sim$ 5% independent of testing temperature as well as tape thickness.

Davies et al (24) give the temperature dependence of superplastic flow as:

$$\dot{\varepsilon} = K_4 d^a \sigma^b \exp(-Q/RT) \qquad \{5\}$$

where K_4 is another constant, d is grain size, the exponent a is in the range $-2>a>-3$, the exponent $b = m^{-1}$, Q is the activation energy for superplastic flow, R is the gas constant, and T is absolute temperature. The flow stress-strain rate data at different temperatures were re-plotted as log σ versus T^{-1} according to the Arrhenius equation {5}, and typical results are shown in figure 3. From equation {5}, the gradient of the Arrhenius plot is - Qm/R, and regression analysis was applied to the log σ - T^{-1} data to obtain values for the activation energy for superplastic flow. The results given in table 2 showed that for each tape thickness, 44 or 75μm, and for each strain rate in the range 10^{-5}..$2.0.10^{-3}s^{-1}$, the activation energy was between 49 and 59kJ $mole^{-1}$ with a correlation coefficient always greater than 0.98. The activation energy had a mean value of 54kJ $mole^{-1}$ with a standard deviation of 3kJ $mole^{-1}$, and was therefore constant within $\sim$ 5% for all strain rates and tape thicknesses. At a given strain rate, the Arrhenius plots for the two tape thicknesses appeared very similar (figure 3) and when regression analysis was applied irrespective of tape thickness the correlation coefficients remained high at >0.97 (last column in table 2). From equation {5} this suggested that the grain size was approximately the same for both tape thicknesses.

Figure 4 shows the microstructure of a melt-spun Pb-Sn eutectic tape observed directly by atomic number contrast in the scanning electron microscope. The high atomic number Pb atoms produce more secondary and back-scattered electrons than the relatively low atomic number Sn atoms. Thus, the microstructure in figure 4 shows equiaxed Pb-rich (light) and Sn-rich (dark) regions $\sim$ 4μm in size. This identification of Pb-rich and Sn-rich regions was confirmed by

scanning X-ray microanalysis, figure 5. The microstructure was similar on both surfaces of each tape and appeared to be independent of tape thickness as had been suggested by the high temperature tensile tests (see last paragraph). This was investigated further by using micrographs such as figure 4 to determine the apparent grain size. On each surface of each specimen the apparent grain size was determined from the mean of 30 measurements of the number of Pb-rich and Sn-rich regions intersected by a 30μm line. The results, given in table 3 showed that the apparent grain size was ∿ 4μm and that it was the same within ∿ 1μm on both tape surfaces, and was independent of tape thickness.

By re-examining the tape surfaces after tensile testing, the deformation process was shown to involve grain boundary sliding as would be expected for superplastic flow. Extensive grain boundary sliding produced the characteristic surface steps shown in figure 6. That these steps were caused by deformation was confirmed by examining an otherwise undeformed tape surface in the region of a Knoop microhardness indent figure 7. With increasing distance from the indent, the number of surface steps decreased because of the decreasing amount of deformation. On micrographs such as figures 6 and 7 steps could be seen at all three types of boundary, ie. Pb-Pb, Pb-Sn and Sn-Sn, indicating that sliding along each type of boundary contributed to the deformation process. The apparent grain size after deformation was measured from micrographs such as figure 6, using the same procedure as that described in the last paragraph. The results, included in table 3, showed that the apparent grain size decreased from ∿ 4μm before deformation to ∿ 3μm after deformation. The main reason for this decrease was that atomic number contrast revealed only Pb-Sn boundaries in the as-solidified microstructure (figure 4); after deformation, a similar number of Pb-Sn boundaries were present, but Pb-Pb and Sn-Sn boundaries could also be seen because of the slip steps produced during grain boundary sliding (figure 6).

Discussion

Previous workers have shown that Pb-Sn eutectic is superplastic when solidified conventionally and then heavily deformed to produce a fine-scale two-phase microstructure (26-29). Avery and Backofen

(27) have quoted the strain rate sensitivity for Pb-Sn eutectic prepared in this way as $\sim$ 0.48 at room temperature when the grain size is $\sim$ 4μm and the strain rate is $10^{-4}s^{-1}$. From the temperature variation of flow stress, Cline and Alden (29) have measured the superplastic activation energy for Pb-Sn eutectic to be $\sim$ 48kJ $mole^{-1}$. The present results show clearly that melt-spun Pb-Sn eutectic tapes exhibit classical superplastic behaviour during tensile deformation. The melt-spun Pb-Sn tapes exhibit a sigmoidal variation of flow stress with strain rate as expected for a superplastic material tested by the cross-head variation technique; the strain rate sensitivity is $\sim$ 0.42 in the strain rate range 10^{-5}-$10^{-3}s^{-1}$, in good agreement with Avery and Backofen's data (27) for conventionally prepared superplastic Pb-Sn tested under comparable conditions; and the activation energy for flow is $\sim$ 54 kJ $mole^{-1}$ also in good agreement with Cline and Alden's data (29) for conventional superplastic Pb-Sn. Two further pieces of evidence support the conclusion that melt-spun Pb-Sn tapes are superplastic. Firstly, microstructural examination of the tape surfaces (figures 4-7) shows that grain boundary sliding is an important deformation mechanism, and this is characteristic of superplastic flow. Secondly, almost all specimens tested to failure in the strain rate range 10^{-5}-$10^{-3}s^{-1}$ exhibit large failure strains of 80-200% and fail by necking to a point as expected for a superplastic material. Tapes cannot extend by more than $\sim$ 200% because of their very small initial thickness (30-120μm), and in a few cases premature failure is initiated at a defect in the unpolished as-solidified tape surface.

There are two possible explanations of the microstructure of melt-spun Pb-Sn eutectic (figure 4) which causes superplastic behaviou during tensile deformation. Either the microstructure is a direct result of the solidification process, or it is caused by post-solidification coarsening. Consider the solidification process first. During melt-spinning, heat is removed from the solidifying tape by radial heat conduction into the rotating copper drum. At a given position along the length of the tape the heat flow is essentially unidirectional, so that the solidification front is approximately parallel to the surface of the drum and moves from the bottom surface of the tape (in contact with the drum) through to the free top surface to complete the solidification process. It is well established (30,31) that during unidirectional solidification eutectic microstructures are determined by two main parameters,

namely the rate of movement of the solidification front R and the temperature gradient at the solid-liquid interface G. Assume that the tape becomes completely solid a distance x from the point of impingement of the liquid stream. The the solidification rate R is given by:

$$R = dV/x \qquad \{6\}$$

where d is the tape thickness and V is the surface velocity of the drum. In the present experiments, $d \sim 50\mu m$, $V \sim 10ms^{-1}$, and the drum diameter D = 150mm. Fully solid tapes can be seen to leave the drum after approximately a tenth of one revolution so that $x \lesssim 50mm$. on the other hand, experiments on higher melting point metals show that the melt pool extends only a few mm from the point of impingement (34,35). Thus the solidification rate R is in the range 10^{-2}-$10^{-1}ms^{-1}$. Previous estimates of solidification rates in other splat-quenching techniques are also in the range 10^{-2}-$10^{-1}ms^{-1}$ (22,32,33). It is more difficult to estimate the temperature gradient during melt-spinning. If there is no barrier to heat flow at the drum-tape interface and if the drum is a perfect heat sink, then the drum-tape interface remains at room temperature T_R. At the point of impingement, as solidification begins the temperature gradient is very high close to the drum-tape interface. As solidification proceeds, the temperature gradient falls until the outer liquid surface reaches the melting point T_M and the temperature gradient is $\sim (T_M-T_R)/d$ i.e. 4.10^6Km^{-1} in the present experiments. The slowest solidification rate is also at the outer surface of the tape so the solidification ratio G/R is $\gtrsim 4.10^8Ksm^{-2}$. Inefficient heat transfer at the drum-tape interface may lead to a somewhat lower figure, say $\sim 4.10^7Ksm^{-2}$. For comparison, table 4 shows values of G,R, and G/R for melt-spinning, directional solidification in a Bridgman crystal grower (36), and small-scale chill-casting (37). It is interesting to notice that G and R are both 10^2-10^3 greater in melt-spinning than in conventional directional crystal growth experiments, but the parameter G/R is approximately the same in both processes.

Directionally solidified Pb-Sn and other simple eutectics such as $Al-Al_2Cu$ have been studied rather extensively (38,40) because of the current interest in using directionally solidified Ni and Co

based eutectics as jet-turbine blade materials (41-43). In a crystal grower with G and R values as in table 4, directionally solidified Pb-Sn, in common with many other eutectics, has a highly regular morphology with alternate lamellae of the two eutectic phases aligned parallel to the heat flow direction (38,39). When G/R falls below a critical value which depends upon the level of ternary impurities. a planar solid-liquid interface becomes unstable, and the lamellae become less well-aligned forming the characteristic wheatsheaf arrangement of eutectic colonies (30). When R is small, the lamellae can become degenerate (30), and the melt-spun Pb-Sn eutectic microstructure seen in both directionally solidified (44) and splat-quenched (45) Al-Al_2Cu eutectic. However, it is unlikely that figure 4 shows a degenerate eutectic microstructure for three reasons. Firstly, degenerate Pb-Sn eutectic usually consists of wavy lamellae rather than the relatively equiaxed microstructure of Al-Al_2Cu (39). Secondly, a degenerate eutectic structure is rather unlikely with the high values of G,R and G/R in melt-spinning (table 4). Thirdly, Cline and Livingston (40) have seen rather different microstructures in Pb-Sn eutectic directionally solidified with $G \gtrsim 10^4 Km^{-1}$ and R as high as $6.10^{-3} ms^{-1}$ i.e. with conditions approaching those in melt-spinning. At high R the region of coupled eutectic growth moved to Sn-rich compositions; thus with $R \gtrsim 3.10^{-3} ms^{-1}$, alloys of eutectic composition solidifed with primary Pb dendrites rather than a fully eutectic microstructure.

It is more likely that the microstructure in figure 4 is formed when the solidification structure coarsens. Lamellar eutectic microstructures are usually very stable even after exposure for long periods at high temperature (46,47). However, the melting point of Pb-Sn eutectic is not very much above room temperature, and quite rapid coarsening has been seen in the degenerate wavy lamellar microstructure (39). Moreover, the coarsening rate can be enhanced very considerably either by the presence of primary dendrites (47) which are expected from Cline and Livingston's experiments (40), or by deformation (48) which might be produced by the shearing effect of the liquid flow during melt-spinning. In the present experiments, an attempt was made to confirm this interpretation by observing a melt-spun Pb-Sn eutectic tape almost immediately after solidification. The microstructure was similar to that in figure 4 but on a much finer scale, which could well indicate a less well developed coarsening of the as-solidified microstructure. Previous experiments on splat-quenched

Pb-Sn eutectic have shown that there is little or no extension of solubility in the two eutectic phases (49,50), and that a metastable hexagonal phase forms when the eutectic is quenched to low temperatures (51,52); however, there have been no reports about the eutectic microstructure. This is currently being investigated further and the results will be described in a future publication.

Acknowledgements

We would like to thank the UK Science Research Council and the US Office of Naval Research (N-00014-78-G-0048) for financial support of this research programme, and Professor R W Cahn for provision of laboratory facilities.

References

1 W Klement Jr, R H Willens & P Duwez: Nature 187 (1960) 809
2 P Duwez, R H Willens & W Klement Jr: J Appl Phys 31 (1960) 1136
3 "International Conference on Metastable Metallic Alloys" Brela Yugoslavia, 1970, Fizika 2 supplement 2 (1970)
4 "Proceedings 2nd International Conference on Rapidly Quenched Metals", Cambridge, Mass, 1975, eds N J Grant & B C Giessen, vol 1 (MIT Press, 1976), vol 2 (Mat Sci Eng 23, 1976, p81-308)
5 H Jones: Rep Prog Phys 36 (1973) 1425
6 T R Anantharaman & C Suryanarayana, J Mat Sci 6 (1971) 1111
7 "Rapidly Quenched Metals III", Proceedings of 3rd International Conference on Rapidly Quenched Metals, Brighton, UK, 1978, ed B Cantor (Metals Society, London, 1978)
8 P Duwez & R H Willens, TMS-AIME 227 (1963) 362
9 R W Cahn, K D Krishananand, M Laridjani, M Greenholz & R Hill in ref (4) vol 2 p 83
10 "Metallic Glasses" (ASM 1978)
11 P Ramachandrao, M G Scott & G A Chadwick, Phil Mag 25 (1972) 96
12 H Jones & C Suryanarayana, J Mat Sci 8 (1973) 705
13 B C Giessen in "Developments in the Structural Chemistry of Alloy Phases" ed B C Giessen (Plenum Press: 1969)
14 G Thomas & R H Willens, Acta Met 12 (1964) 191
15 G Thomas & R H Willens, Acta Met 13 (1965) 139 and 14 (1966) 13
16 Y Inokuti & B Cantor: Scripta Met 10 (1976) 655
17 Y Inokuti & B Cantor: J Mat Sci 12 (1977) 946
18 F Duflos & B Cantor: in ref (7) vol 1 p.110
19 J J Rayment & B Cantor: Met Sci 12 (1978) 156
20 J J Rayment & B Cantor: in ref (7) vol 1 p.85
21 S Kavesh: in ref (10) p.36
22 H Jones: in ref (4) vol 1 p.1
23 B Cantor: to be published
24 S J B Charter, R Cheese & B Cantor, to be published
25 M G Scott: private communication
26 G J Davies, J W Edington, C P Cutler & K A Padmanabhan: J Mat Sci 5 (1970) 1091
27 D H Avery & W A Backofen: Trans ASM 58 (1965) 551
28 P J Martin & W A Backofen: Trans ASM 60 (1967) 352
29 H E Cline & T H Alden: TMS-AIME 239 (1967) 710
30 G A Chadwick: Prog Mat Sci 12 (1963) 97
31 B Cantor: to be published

References Contd.

32 D R Harbur, J W Anderson & W J Maraman: TMS-AIME 245 (1969) 1055
33 M H Burden & H Jones: J Inst Met 98 (1970) 249
34 J L Walter in ref (7) vol 1 p.30
35 H Hillmann & H R Hilzinger in ref (7) vol 1 p.22
36 B Cantor & G A Chadwick: J Cryst G 23 (1974) 12
37 F Jabczynski & B Cantor: in ref (43)
38 R H Hopkins & R W Kraft: TMS-AIME 242 (1968) 1627
39 J D Verhoeven, D P Mower & E D Gibson: Met Trans 8A (1977) 1239
40 H E Cline & J D Livingston: TMS-AIME 245 (1969) 1987
41 "Proceedings of the Conference on In-Situ Composites" pub no. NMAB-308 (National Academy of Sciences, Washington, 1973)
42 "Proceedings of the 2nd Conference on In-Situ Composites" ed M R Jackson, J L Walter, F D Lemkey & R W Hertzberg (Xerox, 1976)
43 "Proceedings of the 3rd Conference on In-Situ Composites" in press
44 T Z Kattamis & M C Flemings, Met Trans 1 (1970) 1449
45 M G Scott, M Kijek & H Matyja, J Mat Sci 13 (1978) 1354
46 L D Graham & R W Kraft, TMS-AIME 236 (1966) 94
47 B Cantor & G A Chadwick, J Cryst G 30 (1975) 140
48 L Y Lin, T H Courtney & K M Ralls, Acta Met 25 (1977) 99
49 I V Salli & I S Miroshnichenko, Dokl Akad Nauk SSR 132 (1960) 557, quoted by ref (12)
50 N I Varich & A A Yakunin, Russ J Phys Chem 41 (1967) 437 quoted by ref (12)
51 R H Kane, B C Giessen & N J Grant, Acta Met 14 (1966) 605
52 I V Salli, V A Dzenzersky, V S Shvets & T Y Evina, Akad Nauk Ukraine SSR Metallofizika 33 (1971) 59, quoted by ref (12

FIGURE CAPTIONS

Figure 1: Variation of flow stress with strain rate for nine thicknesses of melt-spun Pb-Sn eutectic tapes, tensile tested at room temperature.

Figure 2: Variation of flow stress with strain rate for two thicknesses of melt-spun Pb-Sn eutectic tapes, tensile tested at various temperatures.

Figure 3: Arrhenius plots of log flow stress against inverse temperature for two thicknesses of melt-spun Pb-Sn eutectic tapes, tensile tested at various strain rates.

Figure 4: Scanning electron micrographs of (a) top surface and (b) bottom surface of a melt spun Pb-Sn eutectic tape. Dark regions are Sn-rich and light regions are Pb-rich. On both surfaces, the Pb and Sn rich regions are equiaxed, $\sim$ 4μm in size. The bottom surface shows imprints from grooves in the polished copper drum.

Figure 5: Scanning electron micrographs of melt-spun Pb-Sn eutectic tape to confirm interpretation of dark regions as Sn-rich and light regions as Pb-rich (a) secondary electron image (b) Pb Mα X-ray image (c) Sn Lα X-ray image.

Figure 6: Scanning electron micrographs of (a) top surface and (b) bottom surface of a melt-spun Pb-Sn eutectic tape after superplastic deformation. Both surfaces show surface steps caused by grain boundary sliding at Pb-Pb, Sn-Sn, and Pb-Sn boundaries

Figure 7: Scanning electron micrograph of a melt-spun Pb-Sn eutectic tape in the region of a Knoop indent. The number of surface steps decreases with increasing distance from the indent confirming that the steps are caused by deformation.

thickness (μm)	testing temperature T(K)	strain rate sensitivity m	correlation coefficient r	$\log_{10} K_3$
31 ± 2	297	.48	.995	1.86
44 ± 4	297	.42	.998	1.68
	312	.42	.999	1.48
	328	.45	.998	1.43
	334	.45	.997	1.38
	348	.43	.997	1.12
	368	.40	.995	0.87
54 ± 4	297	.40	.996	1.57
58 ± 2	297	.40	.993	1.58
63 ± 3	297	.41	.997	1.63
75 ± 6	297	.40	.999	1.56
	310	.43	.999	1.49
	319	.43	.999	1.36
	324	.42	.998	1.31
	329	.43	.998	1.32
	339	.46	.997	1.31
	342	.45	.997	1.17
	349	.42	.996	1.05
	359	.47	.996	1.06
80 ± 4	297	.42	.994	1.64
92 ± 5	297	.41	.995	1.59
116 ± 11	297	.44	.994	1.64
all specimens, T = 297K		.42	.979	1.63
$\bar{m}$, T = 297K		.42 ± .02		
$\bar{m}$, T > 297K		.43 ± .02		
$\bar{m}$, all specimens		.43 ± .02		

TABLE 1

Strain rate sensitivity of melt-spun Pb-Sn eutectic tapes as a function of tape thickness and testing temperature.

Strain rate $\dot{\varepsilon}$ (s^{-1})	Activation energy for superplastic flow Q, (kJ mole $^{-1}$)			correlation coefficient, r		
	44μm thick tape	75μm thick tape	both 44 and 75μm thick tape	44μm thick tape	75μm thick tape	both 44 and 75μm thick tape
1.2×10^{-5}		56			.989	
2.3×10^{-5}	49	57	53	.998	.983	.971
5.9×10^{-5}	52	59	56	.998	.983	.981
1.2×10^{-4}	55	58	57	.999	.986	.982
2.3×10^{-4}	54	56	55	.999	.990	.984
5.6×10^{-4}	50	52	50	.997	.990	.985
1.0×10^{-3}		50			.989	
2.1×10^{-3}		49			.975	
$\bar{Q}$, all specimens			54 ± 3			

TABLE 2

Activation energy for superplastic flow in melt-spun Pb-Sn eutectic tapes as a function of tape thickness and strain rate.

thickness (μm)	grain size, d(μm)		
	as solidified top surface	as solidified bottom surface	as-deformed
31 ± 2	4.1 ± 1.0	4.2 ± 1.2	2.9 ± 0.6
44 ± 4	3.9 ± 1.0	3.8 ± 0.7	—
54 ± 4	3.9 ± 0.8	3.8 ± 0.8	2.6 ± 0.5
63 ± 3	4.0 ± 0.9	3.3 ± 0.8	—
75 ± 6	4.4 ± 1.2	3.8 ± 1.1	3.5 ± 0.9
80 ± 4	4.0 ± 1.0	4.3 ± 1.0	2.8 ± 0.6
92 ± 5	3.9 ± 1.3	3.6 ± 1.2	2.9 ± 0.7
116 ± 11	4.0 ± 1.0	3.7 ± 1.2	3.2 ± 0.4
$\bar{d}$ (all specimens)	4.0	3.8	3.0

TABLE 3

Grain size in melt-spun Pb-Sn eutectic tapes as a function of tape thickness. The top surface is the surface not in contact with the rotating copper drum during solidification. Each grain size was determined as the mean of 30 measurements of the number of grain intersections along a 30μm line using micrographs such as figures 4 and 5. Scatter bands are given as ± one standard deviation.

solidification process	temperature gradient, G (Km^{-1})	solidification rate, R (ms^{-1})	G/R (Ksm^{-2})
melt-spinning	$\gtrsim 4.10^6$	10^{-2} - 10^{-1}	$\gtrsim 4.10^7$
single crystal growth by directional solidification (36)	10^3	3.10^{-5}	5.10^7
chill-casting (37)	2.10^3	2.10^{-4}	10^7

TABLE 4: Solidification parameters during melt-spinning compared with single crystal growth by directional solidification (36) and chill-casting (37).

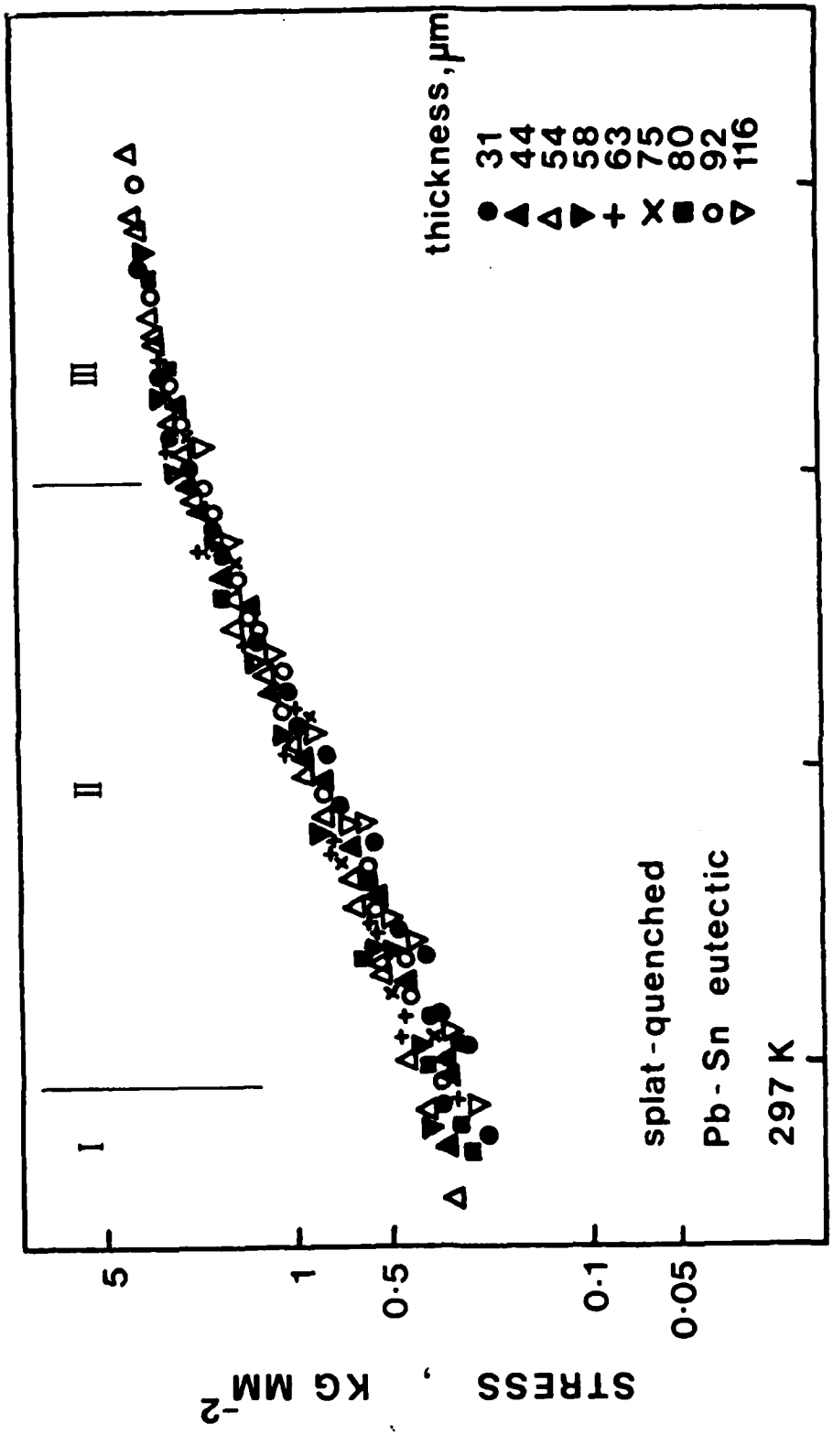
STRESS , KG MM^{-2}
5
1
0·5
0·1
0·05
I
II
III
thickness, μm
31
44
54
58
63
75
80
92
116
splat-quenched
Pb - Sn eutectic
297 K
10^{-5}
10^{-4}
10^{-3}
10^{-2}
STRAIN RATE , S^{-1}

Figure 1

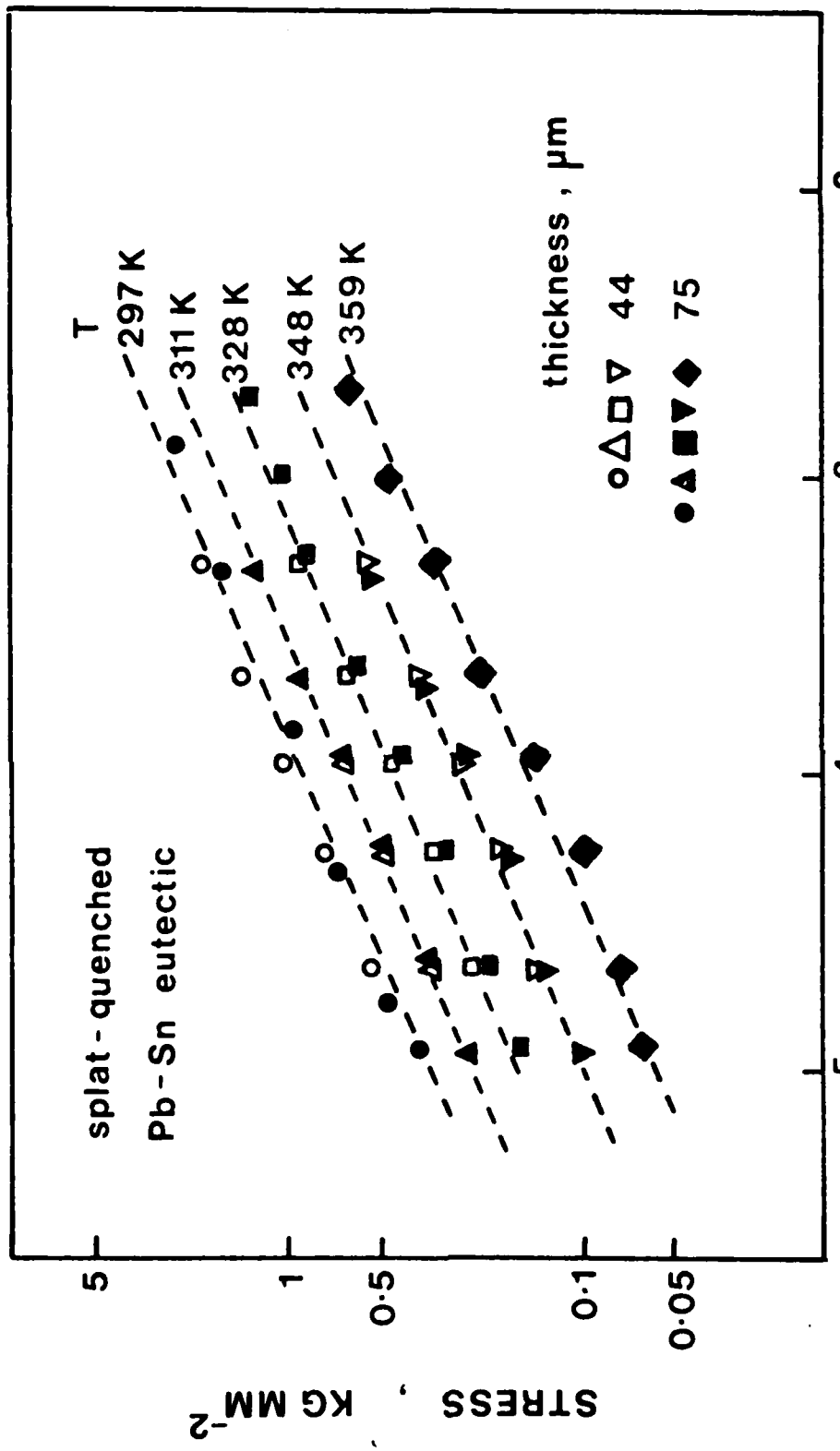
splat-quenched
Pb-Sn eutectic
T
297 K
311 K
328 K
348 K
359 K
thickness, μm
44
75
STRESS, KG MM⁻²
5
1
0·5
0·1
0·05
STRAIN RATE, S⁻¹
10⁻⁵
10⁻⁴
10⁻³
10⁻²

Figure 2

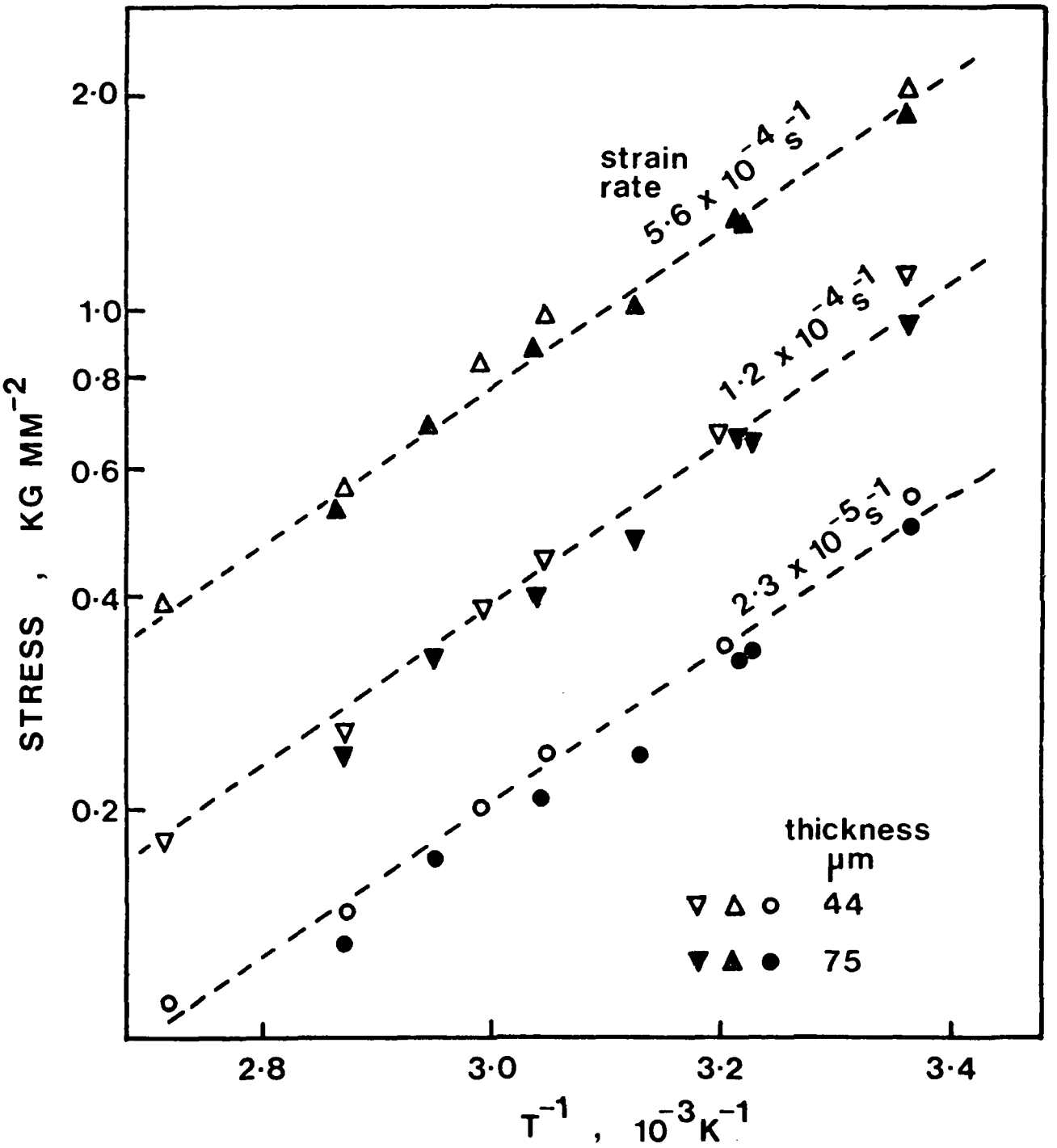
2·0
1·0
0·8
0·6
0·4
0·2
STRESS , KG MM^{-2}
strain rate
5·6 x 10^{-4} s^{-1}
1·2 x 10^{-4} s^{-1}
2·3 x 10^{-5} s^{-1}
thickness μm
44
75
2·8
3·0
3·2
3·4
T^{-1} , 10^{-3}K^{-1}

Figure 3

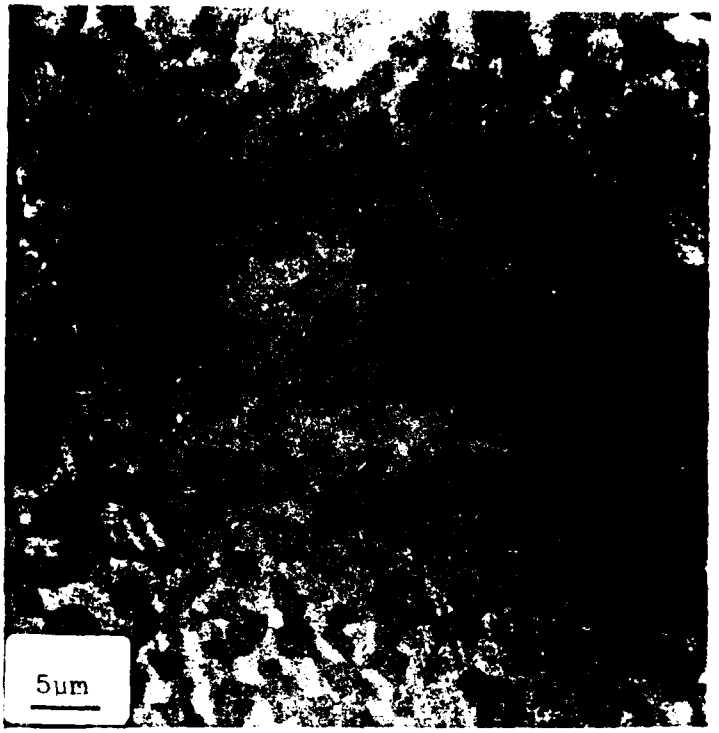
5um

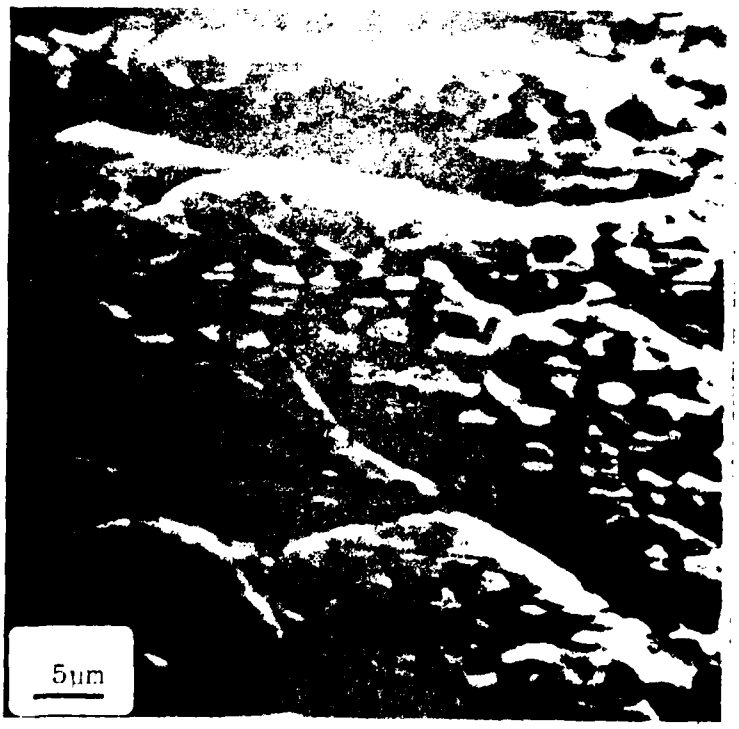
5um

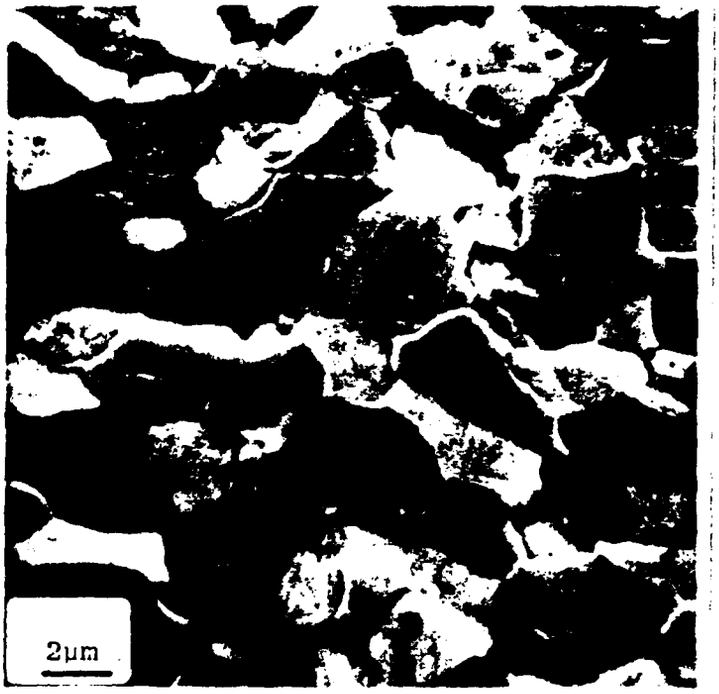

Figure 5(a)

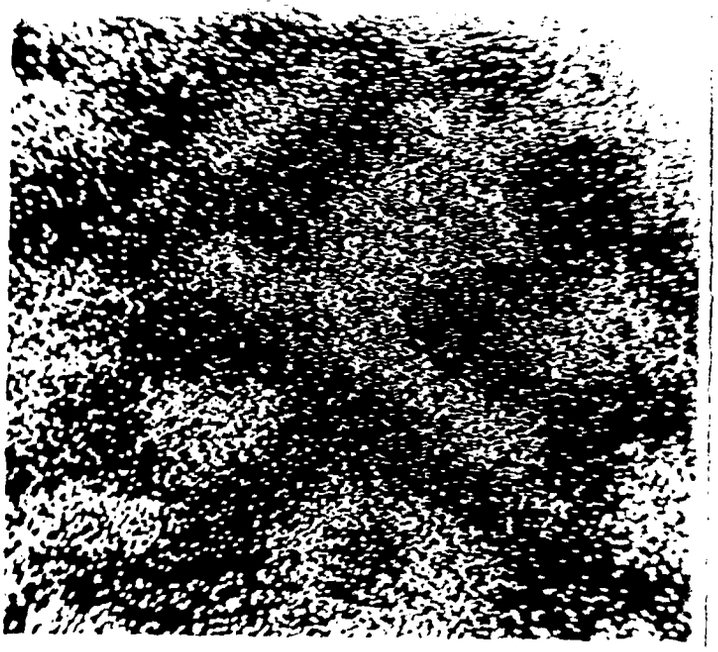

Figure 5(b)

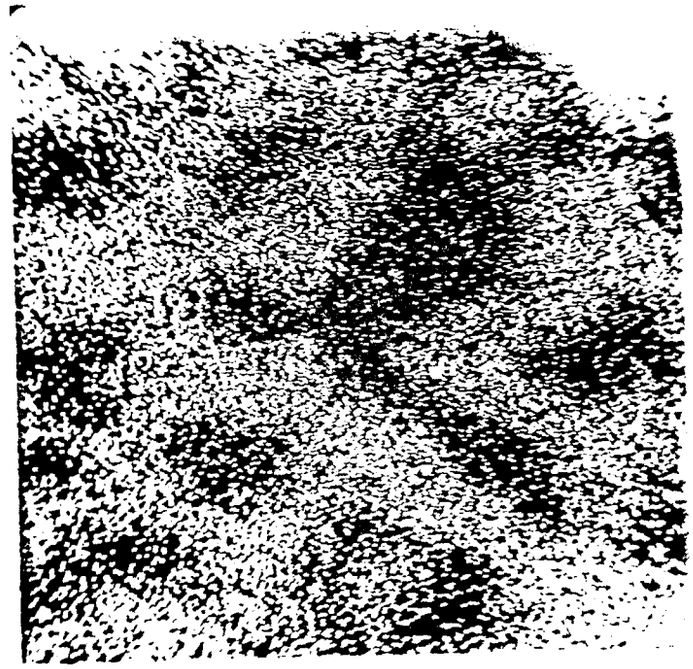

Figure 5(c)

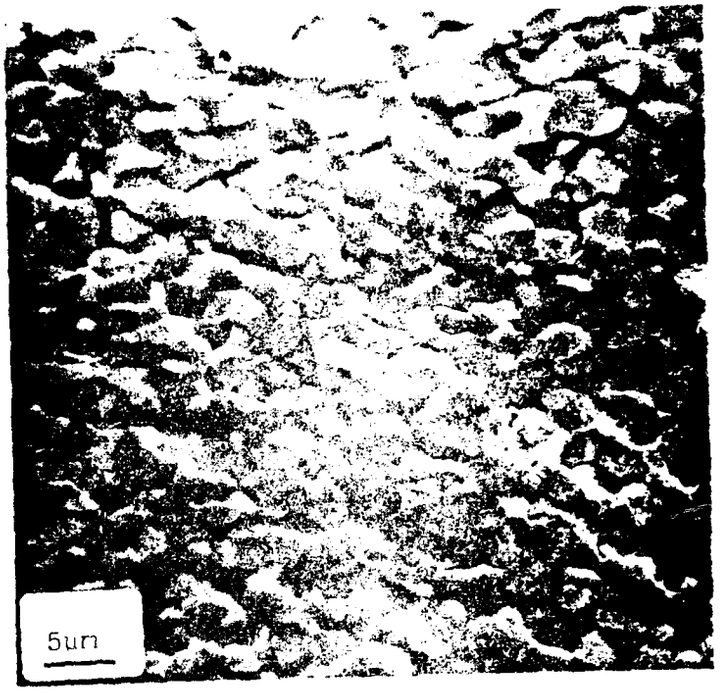

Figure 6(a)

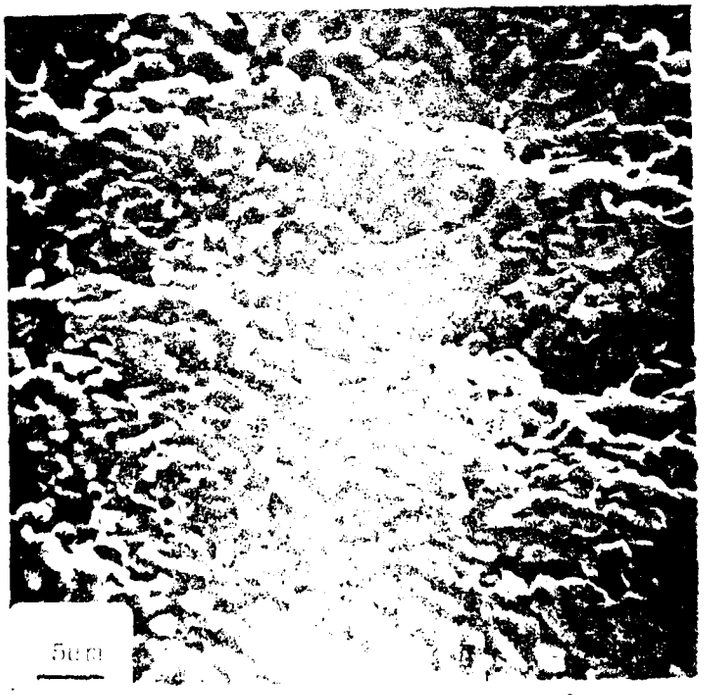

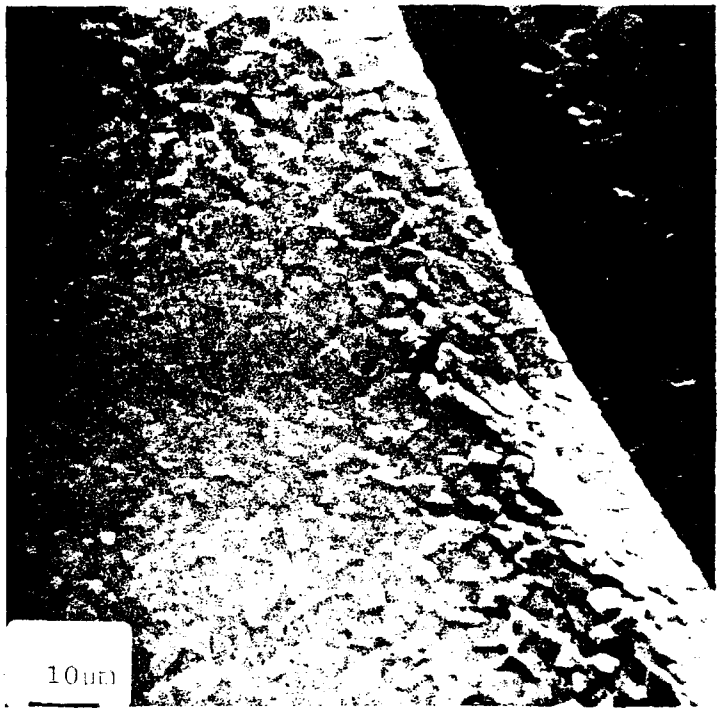

Figure 7


FILMED
8